Journal of Porous Media, 20(7):591–606 (2017)

QUANTIFICATION OF DENSE NONAQUEOUS PHASE LIQUID SATURATION IN DOUBLE-POROSITY SOIL MEDIA USING A LIGHT TRANSMISSION VISUALIZATION TECHNIQUE

Motasem Y. D. Alazaiza,[1] Su Kong Ngien,[1,2,*] Mustafa M. Bob,[3] Samira A. Kamaruddin,[4] & Wan Mohd Faizal Ishak[5]

[1]*Faculty of Civil Engineering and Earth Resources, Universiti Malaysia Pahang, Lebuhraya Tun Razak, 26300, Gambang, Kuantan, Pahang, Malaysia*

[2]*Centre for Earth Resources Research and Management, Universiti Malaysia Pahang, Malaysia*

[3]*Taibah University, College of Engineering, Department of Civil Engineering, Madinah City, Saudi Arabia*

[4]*UTM Razak School of Engineering and Advanced Technology, Universiti Teknologi Malaysia, Malaysia*

[5]*Faculty of Industrial Science and Technology, Universiti Malaysia Pahang, Malaysia*

*Address all correspondence to: Su Kong Ngien, Universiti Malaysia Pahang, Lebuhraya Tun Razak, 26300, Gambang, Kuantan, Pahang, Malaysia, E-mail: nsukong@ump.edu.my

Original Manuscript Submitted: 6/14/2016; Final Draft Received: 9/6/2016

In this research, the light transmission visualization (LTV) technique was used to measure the dense nonaqueous phase liquid (DNAPL) saturation distribution in a two-dimensional (2-D) flow chamber packed with double-porosity soil medium. This, to the best of our knowledge, is a new application of LTV in measuring DNAPL saturation as well as monitoring its migration in double-porosity soil media. The double-porosity structure was created using layers of fine silica sand and solidified kaolin clay spheres. Tetrachloroethylene (PCE) was used to simulate DNAPL and was dyed with Oil-Red-O for better visualization. Known amounts of PCE were injected into the flow chamber before being correlated to amounts calculated using image analysis based on the LTV method. A strong correlation having an R^2 value of 0.994 was found between the injected PCE volumes and calculated PCE volumes obtained from the LTV method. For comparative purposes, the same experiment was carried out by filling the flow chamber with local silica sand as a single-porosity medium to investigate the influence of soil structure on DNAPL migration. Results, again, showed a strong correlation, with an R^2 value of 0.996, between the amounts of PCE injected into the flow chamber and the calculated amounts of PCE. A significant difference in the migration of PCE in the two experiments was observed as the rate of PCE migration in the double-porosity medium was much faster compared to the migration rate in the single-porosity medium. This finding is most likely due to the occurrence of interaggregate pores in the double-porosity soil. This research proves that the noninvasive and nonintrusive LTV technique can be used to quantify DNAPL saturation in double-porosity soil structure in 2-D, two-phase systems.

KEY WORDS: *DNAPL, light intensity, double-porosity, porous media, image analysis, light transmission*

like tetrachloroethylene (PCE) and trichloroethylene (TCE), which are considered as the main types of DNAPLs due to their wide use in the industrial field. When DNAPLs are released into the subsurface, these contaminants will move downward as a separate organic phase, passing through the unsaturated zone. Upon reaching the water table, a DNAPL will penetrate through the water table and continue its downward migration due to its density, which is higher than that of water, before finally becoming immobile on the quasi-aquitard (Zheng et al., 2015). DNAPLs travel through a long migration process, and during these processes, they are usually entrapped in one or several pores as discontinuous ganglia besides accumulating and forming pools (Liang and Falta, 2008). It is very difficult to characterize and remediate sites that have been contaminated by DNAPLs due to their distinct physical and chemical properties. As it is known, fluid flow in porous media plays an important role in many science and engineering applications (Dejam et al., 2015). Consequently, it is necessary to understand and identify the behavior of DNAPL migration as well as its spatial distribution, which will facilitate the design of effective remediation strategies (Bob et al., 2008).

Many factors, such as physical and chemical properties of the DNAPL (O'Carroll et al., 2004), spill rate (Okuda et al., 2014), soil heterogeneity (Yang et al., 2013), and groundwater velocity (Kamon et al., 2004), affect the migration and distribution of DNAPLs in the subsurface. In the natural state, many types of soils have two distinct scales of porosity, which leads to the term *double-porosity* soil structure (Carminati et al., 2008). Double-porosity is a natural phenomenon (El-Zein et al., 2006) found when two separate pore systems occur simultaneously in the structure of the soil. Rock aquifers (Pao and Lewis, 2002), compacted soils (Romero et al., 1999), and agricultural top soil (El-Zein et al., 2006) are examples of geomaterials that potentially harbor double-porosity characteristics.

To understand the contaminant behavior in subsurface systems, it is necessary to produce very high quality data from laboratory experiments, which will be very useful in coming up with an effective remediation technology (Mercer and Cohen, 1990).

Of late, it was found that the migration of fluids within soil can be investigated using image analysis techniques (Sa'ari et al., 2015; Bob et al., 2008; Niemet and Selker, 2001). Generally, these techniques have differences in the absorbance of electromagnetic energy between the different phases, such as liquid, solid, and gas (Niemet and Selker, 2001). The most common examples of these techniques are gamma ray radiation (Oostrom et al., 1998; DiCarlo et al., 1999) , X-ray transmission (Tidwell and Glass, 1994; Rimmer et al., 1998), and light transmission visualization (LTV) (Niemet and Selker, 2001; Bob et al., 2008; Zheng et al., 2015). Gamma rays and X-rays have many limitations, such as the hazard of working with high energy, slow measurements, and high cost. Due to the mentioned limitations, the LTV technique has recently gained in popularity (Weisbrod et al., 2003). A study by Alazaiza et al. (2015) presented the usage of three types of photographic methods in NAPL experiments and showed that LTV is a viable method in NAPL saturation measurements.

LTV requires the least amount of equipment, incurs by far the lowest costs, and does not have hazardous radiation (Wang et al., 2008). The theory behind the LTV technique is the passing of electromagnetic energy into the test media, where the distribution of liquid saturation is measured as variation in the light intensity field. There is a linear relationship between saturation and light intensity due to closer matching between the refraction index of the porous media and water relative to the porous media and air (Glass et al., 1989). In LTV systems, the change in fluid content and fluid saturation can easily be measured instantaneously due to the utilization of cooled charge-coupled device cameras, which provide a very high density array of spatial measurements over a very large dynamic range (Niemet and Selker, 2001).

In general, LTV was developed by Hoa (1981) based on light refraction theory for measuring water content in a sand-filled chamber. Because the relationship between the moisture content and the number of pores filled with water is unknown, an independent calibration curve was needed between saturation and light intensity. After that, Tidwell and Glass (1994) used the LTV technique to measure liquid saturation by correlating the number of pores filled with water to the total number of pores across the thickness of the model and to water saturation. Their method, however, does not need a calibration curve, because the number of pores across the thickness of the model can be calculated for each experiment. Thereafter, Darnault et al. (1998) used the LTV method to investigate the relationship between hue and water content through a full field in a two-phase system (water–oil) using the hue, saturation, and intensity format. They found that the major problem in measuring water and NAPL saturation in the system was the similar refraction indices of these liquids. For that, they used 0.005% FD&C blue dye to color water in a 2-D flow chamber

packed with 12/20 coarse sand. They found that neither saturation nor intensity has a considerable correlation to water content. However, a linear relationship was found between hue and water content, with an R^2 of 0.97. Several years later, Darnault et al. (2001) developed a method to measure fluid content in a three-phase system (NAPL–water–air). They noted that calibration curves need to be generated for each type of sand and each camera used. Niemet and Selker (2001) contributed to LTV by eliminating the need for any empirical parameter determination. Their method was easy to apply, because the number of pores across the thickness can be calculated pixel by pixel from dry and saturated light intensities. Another major contribution to the LTV technique was achieved by Bob et al. (2008), who studied the quantification of PCE saturation in a 2-D, two-fluid-phase system in single-porosity silica sand. Their method did not require a calibration curve in the case of undyed PCE. However, it was necessary to use a single-point calibration step when dyed PCE was used to calculate the change in the transmission factor at the dyed PCE–water interface. They found a very high correlation, with an R^2 value of 0.993, between the known amount of PCE and image analysis results obtained from LTV. In the case of dyed PCE, a stronger correlation ($R^2 = 0.999$) was obtained between the amount of dyed PCE and the results from image analysis.

Research in the field of double-porosity soil structures has gained more attention after a significant discovery by Lewandowska et al. (2005) that showed possible creation of double-porosity characteristics in the laboratory. Lewandowska et al. (2005) carried out a series of one-dimensional infiltration experiments in a column filled with double-porosity soil media. They observed very reasonable quantitative and qualitative agreement between simulations and experimental results. A pioneering study by Ngien et al. (2012) was carried out to investigate the migration of light nonaqueous phase liquid (LNAPL) in double-porosity soil in a one-dimensional circular column using an image analysis technique (light reflection method). Their method needed a calibration curve between the light optical density and LNAPL saturation. Sa'ari et al. (2015) applied the same method used by Ngien et al. (2012) to conduct an experimental study where the migration of LNAPL in double-porosity soil was investigated under different moisture contents of the soil.

In this article, the LTV technique was used to measure DNAPL saturation in double-porosity soil inside a 2-D flow chamber. The method takes into account both absorption and refraction light theories and can directly quantify DNAPL saturation in a two-phase (DNAPL–water) system. The method can accurately measure the distribution of DNAPL saturation in double-porosity soil pixel by pixel, without the need for calibration curves. However, a one-step calibration was required to measure the change in the transmission factor for the dyed DNAPL–water interface. To the best of our knowledge, this is the first attempt to measure DNAPL saturation in double-porosity soil using the LTV technique. For comparison purposes, the same experiment was carried out using only local silica sand to investigate the influence of double-porosity characteristics on DNAPL migration.

This research attempts to bridge the gap as discussed previously by presenting the NAPL saturation calculation and the experiments performed on the migration of DNAPL in double-porosity as well as single-porosity soil. Section 2 presents the materials and method that were used. Light transmission and the saturation calculation in double porosity are presented in Section 3. Section 4 shows the captured images and the results of the image saturation analysis, whereas Section 5 presents the conclusion of the research and possible future work.

2. MATERIALS AND METHODS

2.1 Material Characteristics

The double-porosity media were created using a mixture of spheres made of sintered clay (intra-aggregate pores) and sand (interaggregate pores) following a method described by Lewandowska et al. (2005). The sand used was local silica sand (Lotte Chemical Titan, Malaysia), and the sintered clayey spheres were made from commercially available kaolin S300 (Lotte Chemical Titan, Malaysia). Figure 1 shows the particle size distribution for both silica sand and kaolin S300. The basic physical properties for both sand and kaolin are presented in Table 1. Mineralogical inspection was conducted on the two materials using X-ray diffraction (XRD) to investigate the mineral composition. The main component of the sand was quartz, while the kaolin S300 was mainly composed of kaolinite. Figure 2 shows the XRD results for the two materials.

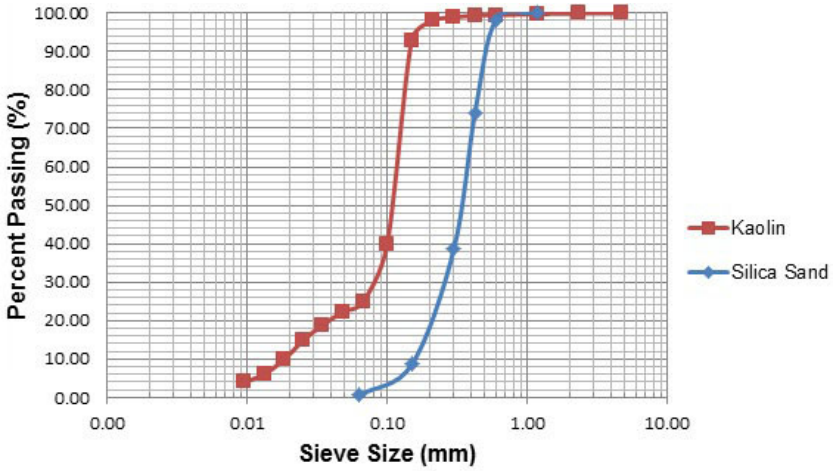

FIG. 1: Particle size distribution of kaolin and silica sand

TABLE 1: Physical properties for S 300 kaolin and silica sand

Material	Test	Parameter	Value
S 300 kaolin	Atterberg limit	Liquid limit	37.1%
		Plastic limit	26.45%
		Plasticity index	10.65%
	Falling head permeability	Coefficient of permeability	8.54×10^{-12} m/s
	Small pyknometer	Density	2.65 kg/m^3
	BET test	Surface area	2.016 m^2/g
Silica sand	Constant head permeability	Coefficient of permeability	4.18×10^{-10} m/s
	Sieve analysis	Mean size, D_{50}	0.32 mm
		Coefficient of uniformity, C_U	2.24
	Small pyknometer	Density	2.69 kg/m^3

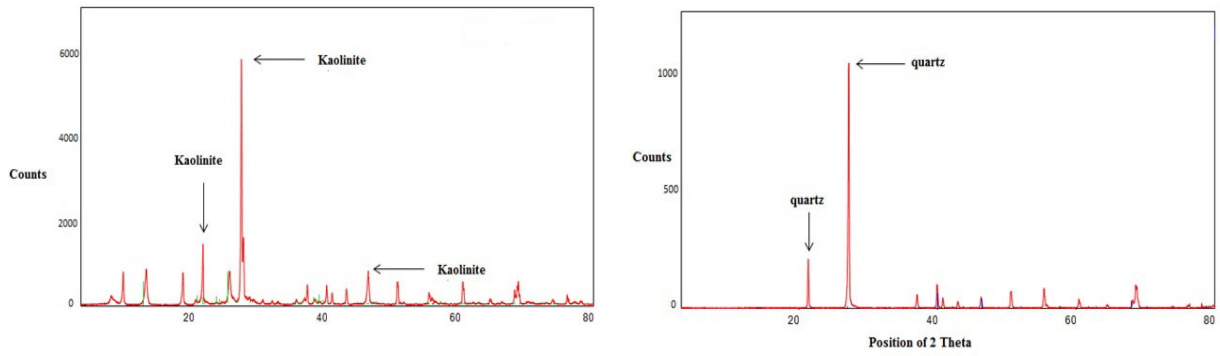

(a) (b)

FIG. 2: XRD chart for (a) kaolin S300 and (b) silica sand

To create the double-porosity structure, a combination of sand and sintered clayey spheres was used. The clayey spheres were made from kaolin powder mixed with a sufficient amount of water before being formed into spheres by hand. The clayey spheres were then put inside the furnace, and the temperature was increased gradually to 1000°C. This process was done to harden the kaolin spheres as well as to decrease the chance of disintegration when the spheres were applied in the saturated phase. The sand was washed with distilled water to remove all the fine residuals that might be present. To further ensure that the sand was clean, the absorption of the waste distilled water that was used to wash the sand was monitored using a spectrophotometer (Hach DR 5000, Arachem (M) Sdn, Bhd, Malaysia). The washing process was continued until the absorption of the waste distilled water was similar to the absorption of the clean distilled water using the same wavelength. Thereafter, the sand was oven dried for 48 hours at 45°C.

2.2 Experimental Setup

The experiments used a 2-D flow chamber made of 10-mm-thick acrylic material with dimensions of 45 cm height $\times$ 30 cm width $\times$ 1 cm depth. The joints of the acrylic flow chamber were sealed together using transparent glue. The flow chamber was kept in a fixed position inside a steel frame that was in turn fixed in a stainless steel light box with dimensions of 65 cm height $\times$ 47 cm width $\times$ 21 cm depth in front of the light source. Two steel ports that were attached to the bottom of the flow chamber allowed the inflow and outflow of fluids. The ports were connected by plastic tubing to a water tank. A steel valve located between the flow chamber and water tank regulated the flow of water into the flow chamber. An inspection was conducted visually to verify that no leakage occurred during the inflow and outflow of water.

The light bank consisted of five 18 W fluorescent tubes (OSRAM, L18W/780 SMARTLUX, Sky White, Malaysia). A holographic light-shaping diffuser (Luminit Torrance, California, USA) was placed behind the flow chamber and in front of the light source to homogenize the light intensity.

Digital images were captured using a Nikon D 7100 digital camera (Nikon, Sdn, Bhd, Malaysia), which was kept at the same distance of 1.5 m from the light box during each of the experimental trials. The camera had 24 megapixels (6000 $\times$ 4000 pixels), resulting in a very high spatial resolution (i.e., each pixel represented approximately 0.07 mm^2 of the chamber surface area). The dynamic range of the camera was 12 bits, resulting in 4096 gray levels. The camera was connected to a laptop, and the image acquisition process was controlled using the Nikon camera control pro software. All images were collected using a 600 nm center-wavelength 10 nm band-pass filter (Orientir Inc., China), which was attached to a 67 mm lens (NIKKOR 18-105 mm f/3.5–5.6G ED VR, Nikon, SDN, BHD, Malaysia). The aperture setting of the lens was adjusted to fully utilize the dynamic range of the camera using exposure times of a few seconds. The aperture of the lens was fixed at $f10$ for all images, and the exposure time was 2 s. The experiments were conducted inside a dark room, and the laboratory environment containing the system was maintained at 23° $\pm$ 1°C. An illustration of the experimental setup is shown in Fig. 3.

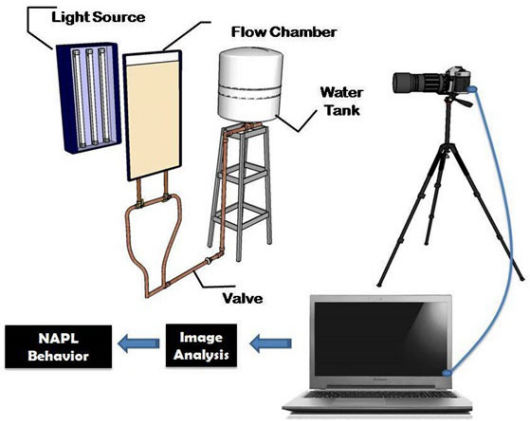

FIG. 3: Experimental setup

2.3 Image Analysis Procedures

After preparing the flow chamber and placing it in front of the light source, the digital camera began capturing the images for quantification of the transmitted light. All images had to be corrected for the temporal variation in the light intensity, as stated by Bob et al. (2008). To carry out correction on the temporal variation in light intensity, a reference image, usually the image captured when the flow chamber is fully saturated with water, was chosen. Two small zones (5×5 cm) on the reference image were identified and referred to as "correction zones." Once the correction zones have been determined, it is very important to ensure that for all other images, these two zones are always fully saturated with water and remain under the same conditions so that any change in light intensity in the correction zones is due to the change in light intensity from the light source. A correction coefficient was identified and calculated from the ratio of the average light intensity of the correction zones for the reference image to the average light intensity of the correction zones of the image that needed to be analyzed. To correct a specific image, the correction coefficient of the image to be corrected was multiplied by the light intensities of the image. For each image collected, it is important to capture three frames consecutively and then take the average value of the light intensities of these three images for calculations. All images were analyzed using Image Pro-Premier 9.1 (Media Cybernetics Inc.). This powerful scientific software has been used by several researchers and provides a convenient direct image processing solution compared to the additional efforts required by other software and programs, such as MATLAB routines. The image analysis procedure is shown in Fig. 4 and was carried out as follows.

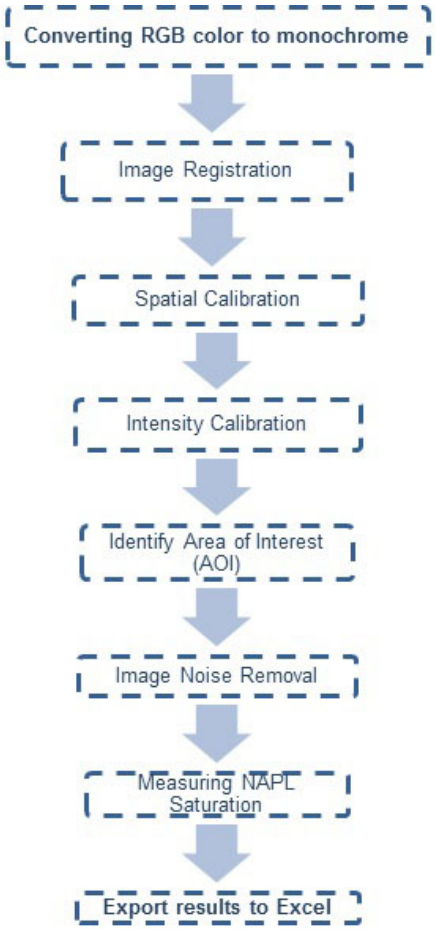

FIG. 4: Image analysis procedures

Initially, the image was converted from red–green–blue (RGB) format to gray level 12 Mono, 12 bpp. This procedure is essential, because RGB produces three channels of pixel image data and contains less valuable image data compared to grayscale, which has only one channel of pixel data. This step is to ensure that the image will produce the full 4096 gray levels present in the image. After that, images with DNAPL plume were registered according to the initial image that was fully saturated with water using the registration tool. This step was done to correct the translation, rotation, and scaling of the images before any measurements on the image were performed. Next, each image was calibrated to the actual measurement using the spatial calibration tool. Performing this calibration ensured that each image was saved in the correct spatial form. After that, all images were calibrated to 12 bit (4096 gray levels) using an intensity calibration tool. This step is ensured that any measurement on the image was calibrated to the actual intensity. The previous two calibrations had to be performed before any image subtraction to ensure that the image subtraction would be performed under the actual spatial relation and intensity.

Following that, the area of interest (AOI) was assigned. AOI refers to the area where all the measurements and calculations will be performed within its boundaries and should be fixed for all the images. Impulse noise was next removed from the image. The image noise is a random variation of brightness or color information in the images. It is usually produced by the sensor of the digital camera. The final step is extracting the intensity in the AOI using Image Bitmap. Through this step, the intensity of the image was translated into a table with columns and rows. Every cell represented one pixel of the image. The table could then be exported to an Excel spreadsheet to calculate the NAPL saturation after deriving the required equations for calculations.

2.4 Experimental Procedures

The procedure to build the double-porosity model was by pouring alternatively a layer of spheres and a layer of sand and then compacting the two layers by tapping the outer frame of the model using a plastic hammer. By following this procedure, the periodic manner could be obtained. After packing the flow chamber with the double-porosity media, the top frame of the flow chamber was closed carefully and sealed with silicon to prevent evaporative losses. The light source was switched on, and after 30 min, the light transmission image for the dry media condition (I_d) was collected. Prior to saturation with water, the packed flow chamber was slowly purged with CO_2 gas through the bottom ports for approximately 40 min. CO_2 is very effective in displacing air and dissolves relatively well in water. After that, the flow chamber was slowly saturated with distilled water from the bottom ports. The saturation process continued until the water level was above the surface of the double-porosity media. Following Niemet and Selker (2001), approximately 1 hour after saturating the flow chamber with water, the saturated transmission image (I_s) was acquired. Known amounts of PCE (Systerm, ChemAR) were injected into the water-saturated flow chamber through the top of the model using an injection needle (syringe). The needle was penetrated into the soil to $\sim$2 cm below the top of the model before the PCE was released. Injection of the PCE was done in seven consecutive amounts (1.0 ml, 1.0 ml, 2.0 ml, 2.0 ml, 2.0 ml, 2.0 ml, and 2.0 ml), where an image after each injection was captured using remote control software. Prior to injecting the PCE, it was dyed with Oil-Red-O dye powder at a concentration of 0.1 g/l. This concentration was found to be sufficient to facilitate good visual observation of the PCE migration through the acrylic wall of the flow chamber. Using a small amount of dye is enough, as reported by Kechavarzi et al. (2000). A spectrophotometer was used to quantify the absorption of the dyed PCE at 600 nm. After image acquisition, the amounts of injected PCE in the flow chamber were calculated based on image analysis, and the results were compared to the actual injected amounts. A mass balance check was then performed to investigate the difference between the calculated amounts of PCE based on image analysis and the actual amount added into the flow chamber.

3. LIGHT TRANSMISSION THROUGH DOUBLE-POROSITY MEDIA

In general, when light passes through different phases of porous media, the light will be absorbed by the different phases, depending on their respective light absorption properties. Light is refracted at the interfaces between the different phases based on the difference in the refractive indices of the phases (Griffiths, 1989). The concept of the equations that was derived to be suitable for the case of double-porosity soil is based on the Bob et al. (2008) equations. Niemet and Selker (2001) proposed that Beer's law (Ryer, 1998) and Fresnel's law (Griffiths, 1989) can be

applied to quantify the absorptive and interfacial light losses when the light is transmitted from phase to phase across the total thickness of the porous media:

$$I = CI_{in}\tau_j \exp\left(-\sum d_i \alpha_i\right) \tag{1}$$

where I is the emergent light intensity, C is the constant for correcting the difference between light observation and light emission (it can be omitted since the camera is approximately the same distance from each light source and the soil media inside the flow chamber), I_{in} is the incident light intensity, τ_j is the transmittance of the interface between the two phases i and $i+1$, $\alpha_i$is the absorption coefficient of the i phase, and d_i is the thickness of the phase i. Equation (1) can be applied to the experimental flow chamber used in this article following the assumption of Bob et al. (2008) that porous media are water-wetting media as well as the assumption that each pore is either full or empty of water, as stated by Tidwell and Glass (1994). By applying Eq. (1) and following Bob et al. (2008) to neglect the visible light absorption by air and water, the following equation is presented, assuming that three phases (air, water, NAPL) are present in the flow chamber:

$$I = I_{in}\tau_{pw}^{2K}\tau_{wa}^{2KX}\tau_{wn}^{2K(1-X-S)} \exp(-\alpha_p d_p k_p - \alpha_n d_o k_n) \tag{2}$$

where τ_{pw} is the transmission factor at the porous media particle–water interface, τ_{wa} is the transmission factor at the water–air interface, τ_{wn} is the transmission factor at the water–NAPL interface, K is the number of pores across the flow chamber thickness, X is the fraction of pores that are filled with air (air saturation), S is the fraction of pores that are filled with water (water saturation), α_p is the absorption coefficient of the porous particles, d_p is the diameter of the porous particles, k_p is the number of porous particles across the thickness of the flow chamber, α_n is the absorption coefficient of the dyed NAPL, d_o is the average pore diameter, and k_n is the number of the pores that are filled with NAPL.

Equation (2) presents the case of a three-phase fluid system. However, in the case where only two phases occur, Eq. (2) can be rewritten with $X = 0$ (i.e., only water and NAPL are present):

$$I = I_{in}\tau_{pw}^{2K}\tau_{wn}^{2K(1-S)} \exp(-\alpha_p d_p k_p - \alpha_n d_o k_n) \tag{3}$$

Equation (3) is valid only in cases where the soil is of single porosity. However, in this research, double-porosity soil is the medium that was studied. Therefore, modifying these equations is necessary for them to be valid and suitable in the case of double porosity. In this research, the case is a two-phase fluid system (i.e., NAPL, water). The main difference will be in the transmission of the light in the presence of double porosity. In the case of single porosity, the light is transmitted through only one type of soil with one porosity. However, in the case of double porosity, as in this research, there are two types of soil with two distinct scales of porosity known as interaggregate and intra-aggregate pores. The light is transmitted through three different interfaces: sand-water interface, clay-water interface, and water-NAPL interface. Therefore Eq. (3) can be rewritten as Eq. (4):

$$I = I_{in}\tau_{sw}^{2k_s}\tau_{cw}^{2k_c}\tau_{wn}^{2(k_s+k_c)(1-S)} \exp(-\alpha_s d_s k_s - \alpha_c d_c k_c - \alpha_n d_o k_n) \tag{4}$$

where τ_{sw} is the transmission factor at the sand particle–water interface, τ_{cw} is the transmission factor at the clay particle–water interface, k_s and k_c are the number of sand particles and clay particles across the thickness of the flow chamber, respectively, α_s is the absorption coefficient for sand particles, d_s is the diameter of sand particles, d_c is the diameter of clay particles, and α_c is the absorption coefficient for clay particles.

In the case where the flow chamber is fully saturated with water, substituting $S = 1$ in Eq. (4) results in Eq. (5), where I_s represents the light intensity for each pixel:

$$I_s = I_{in}\tau_{sw}^{2K_s}\tau_{cw}^{2K_c} \exp(-\alpha_s d_s k_s - \alpha_c d_c k_c) \tag{5}$$

In the case where the flow chamber is fully saturated with NAPL, substituting $S = 0$ in Eq. (4) results in I_N, which presents the light intensity at each pixel under this saturation:

$$I_N = I_{in}\tau_{sw}^{2K_s}\tau_{cw}^{2K_c}\tau_{cw}^{2(K_s+K_c)} \exp(-\alpha_s d_s k_s - \alpha_c d_c k_c - \alpha_n d_o K) \tag{6}$$

Dividing Eq. (6) by Eq. (5) results in an expression of I_N as a function of I_s:

$$I_N = I_s \tau_{wn}^{2[k_s+k_c]} \exp(-\alpha_n d_o K) \tag{7}$$

Equation (7) was used to calculate the theoretical I_N, pixel by pixel, for the model, because it is too difficult and not practical to fully saturate the flow chamber with NAPL each time the model is packed. Dividing Eq. (7) by Eq. (4) to eliminate I_{in} results in

$$I = I_N \tau_{wn}^{-2S[k_s+k_c]} \exp(-\alpha_n d_n k_n + \alpha_n d_o K) \tag{8}$$

The flow chamber contains clay sphere pores (k_c) and sand pores (k_s). Therefore it can be considered that K is the sum of k_s and k_c. Substituting the term K instead of $k_s + k_c$ into Eq. (8) gives

$$I = I_N \tau_{wn}^{-2SK} \exp(-\alpha_n d_n k_n + \alpha_n d_o K) \tag{9}$$

By substituting Eq. (7) into Eq. (9) and arranging the equations, the S_N (NAPL saturation) term at each pixel can be derived:

$$S_N = \frac{\ln I_s - \ln I}{\ln I_s - \ln I_N} \tag{10}$$

From Eq. (10), NAPL saturation can be calculated accurately pixel by pixel in double-porosity soil media for a two-phase system (NAPL–water) without the need to use a calibration curve.

The total number of pores across the thickness of the whole flow chamber (k_s, k_c) can be determined for both clayey spheres and sand, as proposed by Niemet and Selker (2001):

$$k_s = \frac{\ln (I_s/I_d)}{2 \ln (\tau_{sw}/\tau_{pa})} \tag{11}$$

$$k_c = \frac{\ln (I_s/I_d)}{2 \ln (\tau_{cw}/\tau_{pa})} \tag{12}$$

By using Fresnel's law, the transmission factor τ can be calculated between any two phases by measuring the refractive index (n) of these two phases using Eq. (13):

$$\tau = \frac{4 n_1 n_2}{(n_1 + n_2)^2} \tag{13}$$

The refractive index value is 1 for air, 1.6 for sand, 1.33 for water (Tidwell and Glass, 1994; Niemet and Selker, 2001), and 1.56 for kaolin (Ghosh et al., 1990). These values can be used to calculate the transmission factors for the different interphases. In addition, the transmission coefficient for water–NAPL τ_{wn} can be calculated similarly to the sand/clay–water/air interfaces using a PCE refractive index of 1.501 (Bob et al., 2008).

For Eq. (7), it is also needful to measure the absorption coefficient for dyed PCE (α_n), which can be measured using a spectrophotometer. Furthermore, the pixel averaged pore diameter (d_o) can be calculated as shown in Eq. (14) by dividing the total length of the voids by K, where Ø is the sum of the porosities of the soil sample (interaggregate and intra-aggregate), L is the length of the flow chamber, W is the width of the flow chamber, and D is the depth of the flow chamber. The total length of voids across the thickness can be calculated by multiplying the thickness of the model by porosity:

$$d_o = \frac{\phi \times (L \times W \times D)}{K} \tag{14}$$

4. RESULTS AND DISCUSSION

4.1 PCE Saturation in Double-Porosity Soil

Experiment 1 focused on quantifying PCE saturations in 2-D two-phase systems in double-porosity soil media. Different amounts of PCE were injected into the flow chamber (i.e., 1.0 ml, 2.0 ml, 4.0 ml, 6.0 ml, 8.0 ml, 10.0 ml, 12.0 ml). These PCE increments were cumulative (i.e., every time adding 2 ml, except for the starting increment).

Because the PCE was dyed using Oil-Red-O, the absorption process and the light refraction have a significant effect when determining PCE saturations. When the PCE is dyed, it results in reduction of the light transmission in the flow chamber. For PCE saturation calculations, important parameters were calculated and are shown in Table 2.

As mentioned earlier, the transmission factor for the colored PCE–water interface (τ_{wn}) was unknown because the influence of the dye on the light refraction at the PCE–water interface was unknown. Therefore mass balance calibration was used to determine the transmission factor for the colored PCE–water interface (τ_{wn}). For this purpose, in the initial image that was captured after the initial increment of PCE (1.0 ml of PCE), τ_{wn} was calibrated when I_N was calculated to give the exact amount of the injected volume of PCE (i.e., equal to 1.0 ml). Then, the value of τ_{wn} was used in all subsequent calculations. The value of τ_{wn} obtained for the PCE–water interface was 0.993. The injected volume of PCE was plotted against the calculated volume of PCE from image analysis, as shown in Fig. 5. A strong correlation was found between the injected and calculated volumes of PCE ($R^2 = 0.994$). To calculate the overall deviation of the calculated PCE volumes from the injected, the root-mean-square error (RMSE) as given in Eq. (15) was used:

$$\text{RMSE} = \sqrt{\frac{1}{N}\sum (V_{\text{cal}} - V_{\text{inj}})^2} \tag{15}$$

where N is the number of PCE increments, V_{cal} is the calculated PCE volume from image analysis, and V_{inj} is the injected PCE volume. From the calculation, an RMSE value of 0.47 ml was found for the calculated data. As shown in Fig. 5, the image of the initial PCE increment (1.0 ml) was excluded from the graph, because it was used to calibrate the transmission factor for the colored PCE–water interface.

Many types of error that influence the light intensity measurements have been reported by several researchers (e.g., Tidwell and Glass, 1994; Bob et al., 2008). Errors in the measurements of light intensity are usually the result of the nonuniform variations in light source intensity as well as noise in the camera signal. Improving the stability of the light source can reduce the errors resulting from the variations in light source intensity. As Tidwell and Glass (1994) suggested, it is possible to improve the stability of the light source by minimizing the number of times the light source turned on and off. In our experiments, the variation in light intensity was minimized by switching on the light source approximately 30 min before the start of the image acquisition and leaving it turned on during the whole

TABLE 2: Important parameters calculated for experiments

Experiment	Porosity	*K*	Absorption coefficient (α_o)	Average pore diameter (d_o)	Transmission factor (τ_{wn})
1	0.39	51.27	0.260	0.0057	0.993
2	0.33	36.2	0.172	0.0065	0.9965

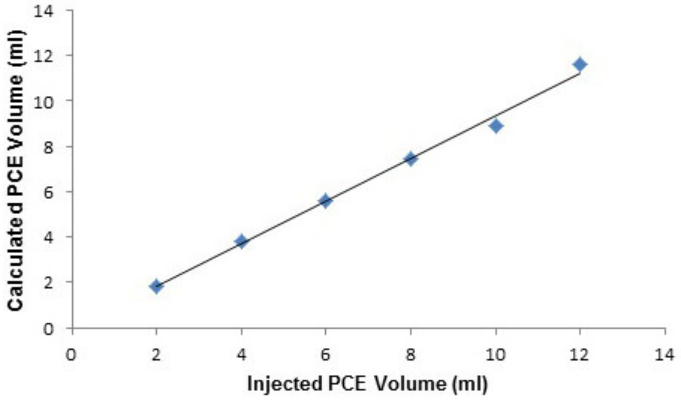

FIG. 5: Injected PCE volume versus calculated volume from image analysis for double-porosity soil, where the solid line represents the best-fit line

duration of the experiments. Light-emitting diodes were also used as a more stable light source (Bob et al., 2008). Because noise in the camera signal existed in every pixel, it is believed that its influence does not affect the mass balance calculation, because it averages out in the summation of all pixels (Niemet and Selker, 2001).

On top of the two aforementioned factors, other factors may contribute to the error in mass balance calculation in this experiment. The conceptual model that was used to calculate the PCE saturation is one possibility. In the conceptual model, it was assumed that each pore was either full or empty of PCE, and this may not necessarily be the case. In reality, it is possible that only a small fraction of the pore volume was filled with PCE, which in turn resulted in an underestimation of PCE volumes by image analysis. Moreover, the conceptual model supposes that inside the flow chamber, the average pore diameter is the same, whereas in reality, the pore diameters are varied, especially in clayey spheres. All previous factors mentioned may contribute to errors in the mass balance calculation.

After calculation of PCE saturations, Surfer software was used to visualize the contour map of the PCE migration. Figure 6 portrays the PCE saturation distribution after 5 min, 10 min, 30 min, and 60 min. In the first 5 min, the PCE

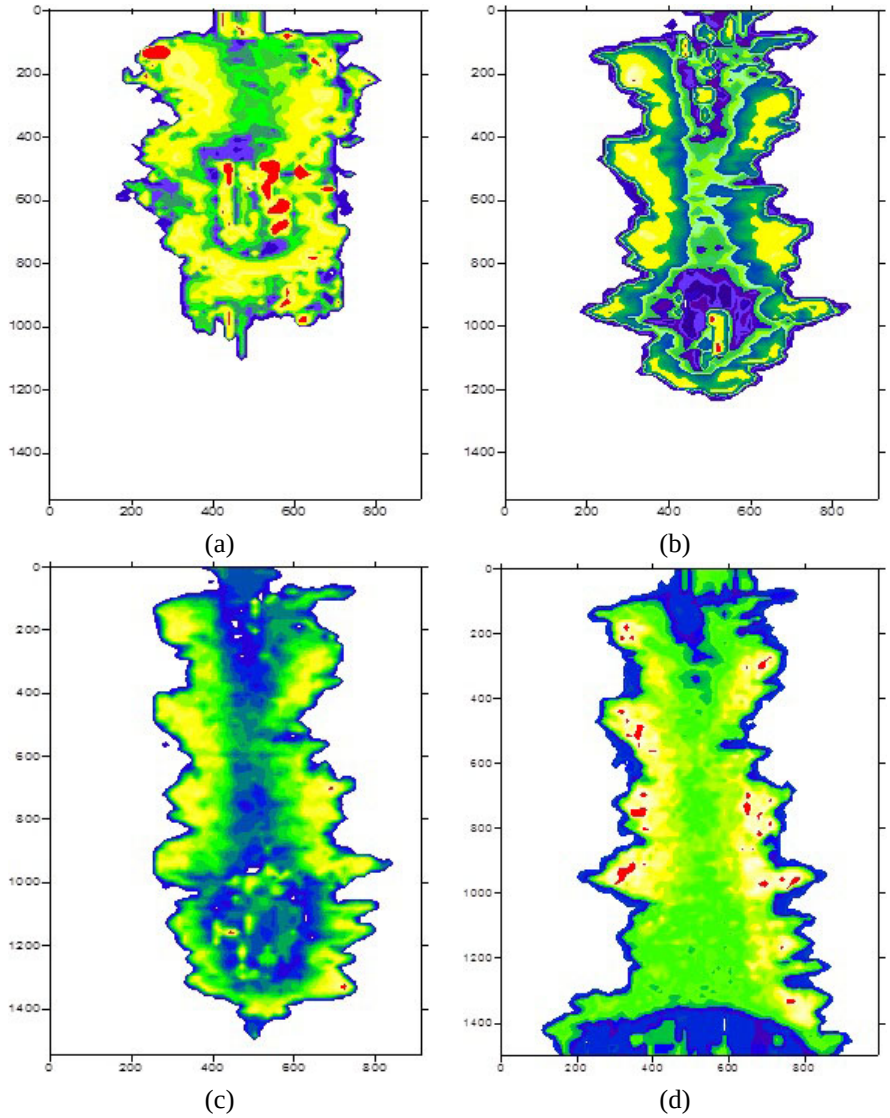

FIG. 6: PCE saturations in double-porosity soil after (a) 5 min, (b) 10 min, (c) 30 min, and (d) 60 min

migration was very fast, reaching nearly halfway through the double-porosity sample, as can be seen in Fig. 6(a). After 5 min, PCE velocity slowed down significantly and reached the bottom of the flow chamber after 34 min, before migrating horizontally across the bottom of the flow chamber. This behavior is in agreement with Sa'ari et al.'s (2015) study. The authors reported in their study that LNAPL migrated much faster in the top layers of the soil due to more interaggregate pores at the top layers of the flow chamber when an uneven compression occurred in the top layers.

4.2 PCE Saturation in Single-Porosity Soil

The second experiment was conducted following the same procedure as in experiment 1. The sole difference is that for experiment 2, the flow chamber was filled with only silica sand to investigate the influence of the double-porosity characteristics found in experiment 1 on the migration of PCE. Important parameters used in the calculations are presented in Table 2. In this experiment, the same equation used by Bob et al. (2008) was used for the PCE saturation calculation, because the porous medium is of single porosity. For mass balance calculation, the findings were in agreement with experiment 1, where a strong correlation was found between the injected volume of PCE and the calculated amount of PCE from image analysis ($R^2 = 0.996$), as shown in Fig. 7. The overall deviations of the calculated PCE volumes from the injected volumes were also calculated, and the RMSE value was found to be 0.56 ml in this experiment.

From the calibration step, the value of transmission factor τ_{wn} obtained for the PCE–water interface was 0.9965, which is higher than that from the double-porosity case. As mentioned earlier, the absorption process has a significant effect on PCE saturation calculations, with many factors influencing the absorption process. One of these factors is the average pore diameter (d_o), which is different for single- and double-porosity mediums. It is believed that the light intensity through the flow chamber was reduced due to the different interfaces that resulted from the composition of double-porosity soil, which in turn caused a decrease in transmission factor under double-porosity conditions compared to single-porosity conditions.

PCE behavior under single-porosity conditions is different from that found with double porosity. It was clear that the velocity of the PCE in sand is very small compared to the velocity with double porosity. The PCE migrated roughly 7 cm during 10 min of injection, whereas within the same duration in double-porosity soil, it traveled more than half of the height of the flow chamber. Basically, the two experiments were conducted under the same conditions, with the same PCE volumes and flow chamber dimensions, with the only difference being the type of medium used. We believe that the main factor that influenced the PCE velocity is the porous media. Interaggregate pores in double-porosity soil,

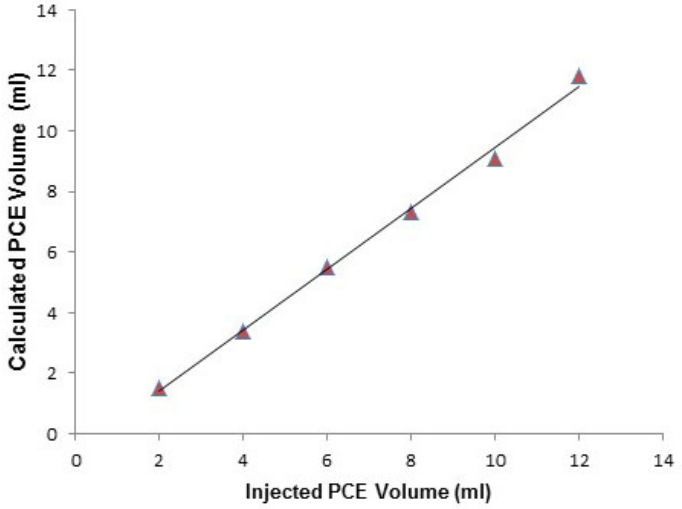

FIG. 7: Injected PCE volume versus calculated volume from image analysis for single-porosity soil

which constitute the main difference in the composition of single and double porosity, have a substantial effect on the migration of PCE. This observation is in agreement with the findings of Ngien et al. (2012), who conducted an experimental study for LNAPL migration in a 1-D column filled with double-porosity aggregated kaolin and compared their results with a study by Alias (2003), who conducted the same experiment using single-porosity, poorly graded sand. Ngien et al. (2012) reported that LNAPL migrated much faster in double-porosity media compared to single-porosity media, and this is due to the occurrence of interaggregate pores. Figure 8 depicts PCE velocity in single- and double-porosity soil carried out in this study.

An interesting phenomenon of PCE flow behavior in the single-porosity soil was observed after 1 hour of migration. Some PCE portions appeared in the two corners at the bottom of the flow chamber. This behavior could be due to uneven compaction of the sand layers, and it might also be that some PCE fractions migrated faster at the back of the flow chamber and then appeared at the bottom. Another unexpected but interesting phenomenon in the single-porosity experiment was that when the PCE reached the bottom of the flow chamber, it climbed up the sides of the flow chamber against gravity, as can be seen in Fig. 9(d). A similar occurrence was also observed by Bob et al. (2008). The method presented here provides a useful tool to measure the changes in DNAPL saturation in double-porosity soil in two-phase systems.

5. CONCLUSION

This article presented the quantification of DNAPL distributions in double-porosity soil in 2-D experimental models using the LTV technique. The method does not need calibration curves to measure the saturations, and it can easily calculate DNAPL saturation pixel by pixel. A strong correlation was found between the actual volumes of PCE injected into the model and the calculated volumes of PCE from image analysis, with an R^2 value of 0.994 in the double-porosity soil experiment. The same experiment was carried out by filling the flow chamber with local silica sand as a single-porosity soil sample for comparative purposes. The findings show that PCE migration was much faster in the double-porosity medium compared to the single-porosity medium. This phenomenon is likely due to the interaggregate pores present in the double-porosity soil, which contributed to an increase in the velocity of fluids. The results of this study show that LTV can provide high-spatial-resolution data for DNAPL saturation measurements in double-porosity soil in two-fluid-phase systems. This method can be developed to measure NAPL saturations in three-fluid-phase systems (NAPL–water–air).

ACKNOWLEDGMENTS

This research was funded by the Fundamental Research Grant Scheme (project RDU 130139) from the Ministry of Higher Education, Malaysia, led by the second author. Also, the authors are grateful for support from University Malaysia Pahang (UMP) to the first author.

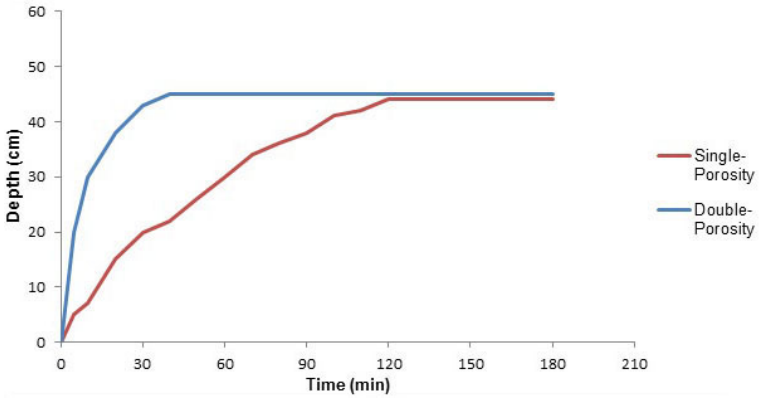

FIG. 8: PCE migration in double- and single-porosity soils

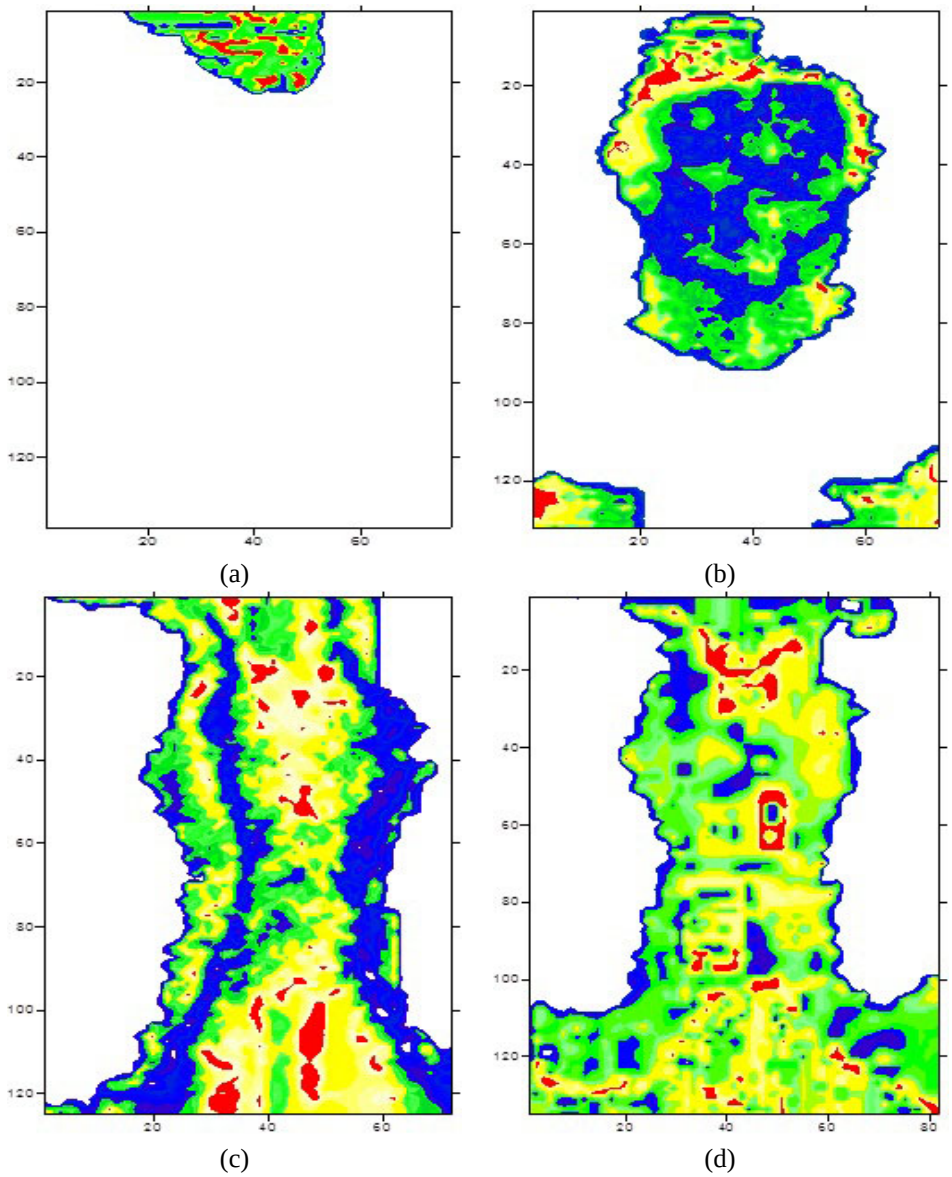

FIG. 9: PCE saturations in single-porosity soil after (a) 10 min, (b) 60 min, (c) 120 min, and (d) 180 min

REFERENCES

Alazaiza, M.Y.D., Ngien, S.K., Bob, M.M., Ishak, W.M.F., and Kamaruddin, S.A., An overview of photographic methods in monitoring non-aqueous phase liquid in porous meduim, *Spec. Topics Rev. Porous Media*, vol. **6**, no. 4, pp. 367–381, 2015.

Alias, N., Migration of Light Nonaqueous Phase Liquid (LNAPL) in Unsaturated Media, MEng thesis, Universiti Teknologi Malaysia, 2003.

Bob, M.M., Brooks, M.C., Mravik, S.C., and Wood, A.L., A modified light transmission visualization method for DNAPL saturation measurements in 2-D models, *Adv. Water Resour*., vol. **31**, pp. 727–742, 2008.

Carminati, A., Kaestner, A., Lehmann, P., and Flühler, H., Unsaturated water flow across soil aggregate contacts, *Adv. Water. Resour.*, vol. **31**, pp. 1221–1232, 2008.

Darnault, C., Dicarlo, D., Bauters, T., Jacobson, A., Throop, J., Montemagno, C., Parlange, J.Y., and Steenhuis, T., Measurement of fluid contents by light transmission in transient three-phase oil-water-air systems in sand, *Water Resour. Res.*, vol. **37**, pp. 1859–1868, 2001.

Darnault, C.J., Throop, J.A., Dicarlo, D.A., Rimmer, A., Steenhuis, T.S., and Parlange, J.-Y., Visualization by light transmission of oil and water contents in transient two-phase flow fields, *J. Contam. Hydrol*., vol. **31**, pp. 337–348, 1998.

Dejam, M., Hassanzadeh, H., and Chen, Z., Capillary forces between two parallel plates connected by a liquid bridge, *J. Porous Media*, vol. **18**, no. 3, pp. 179–188, 2015.

Dicarlo, D.A., Bauters, T.W., Darnault, C.J., Steenhuis, T.S., and Parlange, J., Lateral expansion of preferential flow paths in sands, *Water Resour. Res.*, vol. **35**, pp. 427–434, 1999.

El-Zein, A., Carter, J.P., and Airey, D., Three-dimensional finite elements for the analysis of soil contamination using a multiple-porosity approach, *Int. J. Numer. Anal. Model*., vol. **30**, pp. 577–597, 2006.

Ghosh, S., Warrier, K., and Damodaran, A., Thermally treated kaolin as an extender pigment, *J. Mater. Sci. Lett.*, vol. **9**, pp. 1046–1048, 1990.

Glass, R.J., Steenhuis, T.S., and Parlange, J.-Y., Mechanism for finger persistence in homogeneous, unsaturated, porous media: Theory and verification, *Soil Sci*., vol. **148**, pp. 60–70, 1989.

Griffiths, D.J., *Introduction to Electrodynamics*, Englewood Cliffs, NJ: Prentice-Hall, 1989.

Hoa, N., A new method allowing the measurement of rapid variations of the water content in sandy porous media, *Water. Resour. Res.*, vol. **17**, pp. 41–48, 1981.

Kamon, M., Endo, K., Kawabata, J., Inui, T., and Katsumi, T., Two-dimensional dnapl migration affected by groundwater flow in unconfined aquifer, *J. Hazard Mater.*, vol. **110**, pp. 1–12, 2004.

Kechavarzi, C., Soga, K., and Wiart, P., Multispectral image analysis method to determine dynamic fluid saturation distribution in two-dimensional three-fluid phase flow laboratory experiments, *J. Contam. Hydrol*., vol. **46**, pp. 265–293, 2000.

Lewandowska, J., Szymkiewicz, A., Gorczewska, W., and Vauclin, M., Infiltration in a double-porosity medium: Experiments and comparison with a theoretical model, *Water Resour. Res*., vol. **41**, W02022, 2005, DOI:10.1029/2004WR003504.

Liang, H. and Falta, R.W., Modeling field-scale cosolvent flooding for DNAPL source zone remediation, *J. Contam. Hydrol*., vol. **96**, pp. 1–16, 2008.

Mercer, J.W. and Cohen, R.M., A review of immiscible fluids in the subsurface: Properties, models, characterization and remediation, *J. Contam. Hydrol*., vol. **6**, pp. 107–163, 1990.

Ngien, S.K., Rahman, N.A., Bob, M.M., Ahmad, K., Sa'ari, R., and Lewis, R.W., Observation of light non-aqueous phase liquid migration in aggregated soil using image analysis, *Transp. Porous Media*, vol. **92**, pp. 83–100, 2012.

Niemet, M.R. and Selker, J.S., A new method for quantification of liquid saturation in 2D translucent porous media systems using light transmission, *Adv. Water Resour*., vol. **24**, pp. 651–666, 2001.

O'Carroll, D.M., Bradford, S.A., and Abriola, L.M., Infiltration of PCE in a system containing spatial wettability variations, *J. Contam. Hydrol*., vol. **73**, pp. 39–63, 2004.

Okuda, N., Shimizu, T., Muratani, M., Terada, A., and Hosomi, M., Study of penetration behavior of PCB-DNAPL in a sand layer by a column experiment, *Chemosphere*, vol. **114**, pp. 59–68, 2014.

Oostrom, M., Hofstee, C., Dane, H., and Lenhard, R.J., Single-source gamma radiation procedures for improved calibraion and measurements in porous media, *Soil Sci*., vol. **163**, pp. 646–656, 1998.

Pao, W.K. and Lewis, R.W., Three-dimensional finite element simulation of three-phase flow in a deforming fissured reservoir, *Comput. Methods Appl. Mech*., vol. **191**, pp. 2631–2659, 2002.

Rimmer, A., Dicarlo, D.A., Steenhuis, T.S., Bierck, B., Durnford, D., and Parlange, J.-Y., Rapid fluid content measurement method for fingered flow in an oil–water–sand system using synchrotron X-rays, *J. Contam. Hydrol*., vol. **31**, pp. 315–335, 1998.

Romero, E., Gens, A., and Lloret, A., Water permeability, water retention and microstructure of unsaturated compacted boom clay, *Eng. Geol*., vol. **54**, pp. 117–127, 1999.

Ryer, A., *Light Measurement Handbook*, Newburyport, MA: International Light, 1998.

Sa'ari, R., Rahman, N., Yusof, Z., Ngien, S., Kamaruddin, S., Mustaffar, M., and Hezmi, M., Application of digital image processing technique in monitoring LNAPL migration in double porosity soil column, *J. Teknol*., vol. **72**, pp. 23–29, 2015.

Tidwell, V.C. and Glass, R.J., X-ray and visible light transmission for laboratory measurement of two-dimensional saturation fields

in thin-slab systems, *Water Resour. Res*., vol. **30**, pp. 2873–2882, 1994.

Wang, H., Chen, X., and Jawitz, J.W., Locally-calibrated light transmission visualization methods to quantify nonaqueous phase liquid mass in porous media, *J. Contam. Hydrol*., vol. **102**, pp. 29–38, 2008.

Weisbrod, N., Niemet, M.R., and Selker, J.S., Light transmission technique for the evaluation of colloidal transport and dynamics in porous media, *Environ. Sci. Technol*., vol. **37**, pp. 3694–3700, 2003.

Yang, Z., Zandin, H., Niemi, A., and Fagerlund, F., The role of geological heterogeneity and variability in water infiltration on non-aqueous phase liquid migration, *Environ. Earth Sci.*, vol. **68**, pp. 2085–2097, 2013.

Zheng, F., Gao, Y., Sun, Y., Shi, X., Xu, H., and Wu, J., Influence of flow velocity and spatial heterogeneity on DNAPL migration in porous media: Insights from laboratory experiments and numerical modelling, *Hydrogeol. J.*, vol. **23**, pp. 1703–1718, 2015.